PAPER • OPEN ACCESS

Friction-limited cell motility in confluent monolayer tissue

Physical Biology

OPEN ACCESS

PAPER

Friction-limited cell motility in confluent monolayer tissue

RECEIVED
16 January 2018

REVISED
19 June 2018

ACCEPTED FOR PUBLICATION
25 June 2018

PUBLISHED
25 July 2018

Amalie Christensen[1], Ann-Katrine Vrans West[1], Lena Wullkopf[2], Janine Terra Erler[2], Lene Broeng Oddershede[1] and Joachim Mathiesen[1,3]

[1] Niels Bohr Institute, University of Copenhagen, Copenhagen, Denmark
[2] Biotech Research & Innovation Centre (BRIC), University of Copenhagen, Copenhagen, Denmark
[3] Author to whom any correspondence should be addressed.

E-mail: mathies@nbi.ku.dk

Keywords: collective cell motion, mechanical model, substrate friction, tissues

Abstract

Mechanical forces are important factors in the development, coordination and collective motion of cells. Based on a continuum-scale model, we consider the influence of substrate friction on cell motility in confluent living tissue. We test our model on the experimental data of endothelial and cancer cells. In contrast to the commonly used drag friction, we find that solid friction best captures the cell speed distribution. From our model, we quantify a number of measurable physical tissue parameters, such as the ratio between the viscosity and substrate friction.

1. Introduction

Various models of collective cell motion exist in the literature, including particle-based models [1–4], cellular Potts models [5–7], vertex models [8], phase field models [9] and continuum-scale models with [10–16] and without cell polarization [17, 18]. Often, continuum-scale models have the advantage of being analytically more tractable than the corresponding particle-based models. However, a general problem with most models is how to choose the right constitutive relation between quantities, such as cell strain and stress or to decide on the right functional form of various dissipative processes. Observations at the level of individual cells suggest that cell deformation is viscoelastic [19, 20], i.e. at short time scales, any deformation responds elastically to a mechanical loading, whereas loads applied over a longer period will be followed by a viscous relaxation and thus an irreversible deformation.

Several constitutive relations have been employed to describe the deformation of single cells, see, for example, [21]. Examples of such relations include a Maxwell fluid (figure 1(A)), consisting of a dashpot in *series* with a spring, and a Kelvin–Voigt solid (figure 1(B)) consisting of a dashpot in *parallel* with a spring. Depending on the coupling of the basic building blocks (dashpots and springs) a broad range of fluid-like and solid-like behaviors can be obtained. One prominent example of a basic rheological model is the standard linear solid, where the dashpot in the Kelvin–Voigt element is coupled in series with a spring. When subjected to a sudden strain, the stress in the standard linear solid model decays exponentially towards a constant non-zero value.

Aggregates of cells in tissues also behave viscoelastically [22]. Based on stress relaxation experiments on freely suspended cell monolayers, Harris *et al* [23] used the standard linear solid model to estimate an apparent viscosity for Madin–Darby canine kidney cell monolayers. Guevorkian *et al* [24] obtained an apparent viscosity for murine sarcoma cell aggregates using a micropipette aspiration technique and the standard linear solid model in series with a dashpot. Forgacs *et al* [25] performed parallel plate compression experiments on chicken cell aggregates and estimated the viscosity using a rheological model of two parallel-coupled Maxwell fluid elements. In addition, the viscosity of breast cancer tumors has been measured using ultrasonic shear-wave imaging experiments combined with a Maxwell model [26].

2. Methods

We shall here consider the Oldroyd-B rheological model (see, for example, [27]), which follows from the immersion of a Maxwell fluid of viscosity η_1 and shear modulus G in a Newtonian fluid of viscosity η_2 (figure 1(C)). Defining the total viscosity $\eta_0 = \eta_1 + \eta_2$, the relaxation time $\lambda_1 = \eta_1/G$ and the retardation time $\lambda_2 = (\eta_2/\eta_0)\lambda_1$, the Oldroyd-B constitutive relation is:

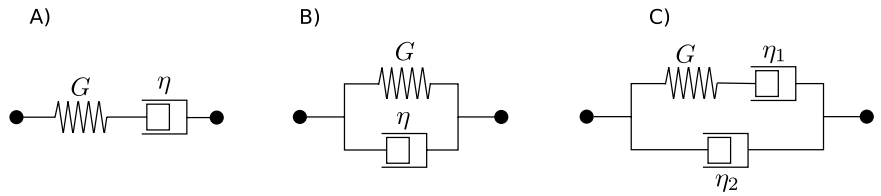

Figure 1. Rheological diagrams. (A) Maxwell fluid. Under sudden stress, the spring of elastic modulus G deforms instantaneously whereas the dashpot deforms at a constant rate like a fluid of viscosity η. When the Maxwell element is released, the spring regains its original length, but the dashpot irreversibly maintains its deformation. (B) Kelvin–Voigt solid. Under sudden stress, the Kelvin–Voigt solid deforms with a characteristic time scale η/G. The deformation is reversible, and, when released, the Kelvin–Voigt solid regains its original shape. (C) Oldroyd-B fluid. When subjected to a sudden strain ϵ_0, the stress decays exponentially with a timescale η_1/G towards zero.

$$\sigma + \lambda_1 \overset{\nabla}{\sigma} = 2\eta_0 \left(\gamma + \lambda_2 \overset{\nabla}{\gamma}\right), \tag{1}$$

where $\overset{\nabla}{\sigma}$ and $\overset{\nabla}{\gamma}$ are the upper convected derivatives of the deviatoric stress tensor σ, $\gamma = \frac{1}{2}(\nabla\mathbf{v} + (\nabla\mathbf{v})^T)$ is the strain rate tensor and $\mathbf{v}$ is the local mean velocity. Experiments measuring the stress relaxation of tissue after a sudden compression have found that the stress relaxes exponentially with one or two characteristic time scales depending on the external loading conditions [23, 25]. The Oldroyd-B model only captures a single characteristic relaxation time scale λ_1 under the same experimental conditions. While more rheological elements could be added to account for more time scales, we shall here aim at simplicity and stick with a description based on a single time scale.

Moreover, the upper convected derivative can often be greatly simplified in slowly moving tissues. Defining a characteristic time t_γ on which γ changes, a characteristic flow speed U_v and length scale L_v, the upper convected derivative can be cast in dimensionless form:

$$\overset{\nabla}{\gamma} = \frac{\partial\gamma}{\partial t} + \frac{t_\gamma U_v}{L_v}\left\{(\mathbf{v}\cdot\nabla)\gamma - \left[\gamma\cdot(\nabla\mathbf{v}) + (\nabla\mathbf{v})^T\cdot\gamma\right]\right\}. \tag{2}$$

In the limit where the time scale, L_v/U_v, used for a fluid element to traverse a length scale L_v, is large compared to the characteristic (relaxation) time t_γ, the quantity $t_\gamma U_v/L_v$ (the Deborah number) is small and the upper convected derivative reduces to a partial derivative with respect to time,

$$\overset{\nabla}{\gamma} \approx \frac{\partial\gamma}{\partial t}. \tag{3}$$

In the experimental data, we shall consider below that the used cell lines have a characteristic flow velocity $U_v \sim 1\,\mu\text{m min}^{-1}$ and a characteristic size of $L_v \sim 20$ μm (see appendix A). The typical relaxation time is of the order of a minute. The prefactor in the upper convected derivative is therefore relatively small $t_\gamma U_v/L_v \sim 0.05$.

2.1. Substrate friction

The friction between motile cells and the substrate is often considered to be linear in the cell velocity [1, 10, 17, 18, 28, 29]. That is, the friction is similar to the viscous drag on a fluid flowing over a surface at low Reynolds numbers. In contrast, measurements on individual cells suggest that the traction force exerted by a cell is non-trivially related to the filmamentous actin speed [30]. The traction force seems to follow an increasing trend for low actin speeds, crossing over to a decreasing trend for larger actin speeds. It remains an open question as to whether these measurements can be generalized to the larger scale dynamics of, for example, a confluent cell layer. From a modelling point of view, various forms of friction can be derived from the dynamics of discrete contact points between cells and the substrate, see, for example [31]. Here, we consider the dynamical consequences of various friction terms using, as a starting point, a simple stochastic differential equation. In conclusion, we find that a term which crosses over to solid friction (or so-called Coulomb friction) for larger velocities offers the best quantitative agreement with our data and is consistent with the experimental observation that the speed distribution of the cells have exponential tails (see figure 3(A)). The Coulomb friction does not depend on the speed, only on the velocity direction $\hat{\mathbf{v}} = \mathbf{v}/|\mathbf{v}|$ scaled with a friction coefficient α.

For simplicity, let us for a moment disregard the interaction between cells and consider only the balance between the motility force and friction force of an individual cell. We first consider the motility force to be a basic stochastic process similar to the Ornstein–Uhlenbeck process, which describes a viscously damped and stochastically-driven particle. This process has also been commonly used to describe cell motion [32, 33]. The process is formulated in the cell velocity $\mathbf{v}$,

$$\frac{d\mathbf{v}}{dt} = \boldsymbol{\psi}(\mathbf{v}) + \boldsymbol{\xi}(t), \tag{4}$$

where the motility force $\boldsymbol{\xi}$ is a Gaussian white-noise field of strength $\langle\xi_i(t)\xi_j(t')\rangle = 2\delta(t-t')\delta_{ij}$ and the friction (or damping) force is given by $\boldsymbol{\psi}(\mathbf{v})$. Note that we have scaled the damping term and time with a general amplitude of the noise field.

If the friction force is assumed to be isotropic and always acts in a direction opposite to the local velocity, it will assume a form

$$\boldsymbol{\psi}(\mathbf{v}) = \psi(v)\hat{\mathbf{v}}. \tag{5}$$

From the stochastic differential equation (4), one obtains the corresponding Fokker–Planck equation for the speed distribution,

$$\frac{\partial P(\mathbf{v},t)}{\partial t} = -\nabla\cdot\left(\boldsymbol{\psi}(\mathbf{v})P(\mathbf{v},t)\right) + \nabla^2 P(\mathbf{v},t). \tag{6}$$

Because of the rotational symmetry of the damping term, the equation only contains the radial term in velocity space, i.e.

$$\frac{\partial P(v,t)}{\partial t} - \frac{\partial}{\partial v}\left(\psi(v)P(v,t)\right) - \frac{\psi(v)P(v,t)}{v} + v\frac{\partial}{\partial v}\left(v\frac{\partial P(v,t)}{\partial v}\right) = 0. \tag{7}$$

We find the stationary distribution $P(v)$ by demanding that the time derivative vanishes, i.e. we have the equation

$$\frac{\partial^2 P}{\partial v^2} + \left(\frac{1}{v} - \psi\right)\frac{\partial P}{\partial v} - \left(\frac{\partial \psi}{\partial v} + \frac{\psi}{v}\right)P = 0. \tag{8}$$

For a given $\psi(v)$, the solution to the steady-state equation can be written in the form

$$P(v) = K\exp\left(\int^v \psi(v')dv'\right) \tag{9}$$

where K is a normalization constant. In the case of Coulomb friction, where for all $v \neq 0$ the term $\psi(v) = -\alpha$ is a constant, the steady-state distribution becomes an exponential

$$P(v) = \alpha\ \exp\left(-\alpha v\right). \tag{10}$$

A stochastic differential equation similar to the one considered here has been suggested to describe the dynamics in granular systems [34].

For completeness, we write the contrasting Gaussian tail achieved when a linear damping term is used, $-\alpha\mathbf{v}$,

$$P(v) = \sqrt{\frac{2\alpha}{\pi}}\exp\left(-\frac{\alpha v^2}{2}\right). \tag{11}$$

At a microscopic level, a velocity-independent friction arising from contact with the substrate would require the contact area of individual cells to be roughly constant, or similarly require the number of bonds formed between a cell and the substrate to be independent of the cell velocity. For this to be the case, the rate of bond formation and breakage would have to be equal. In dry friction [35], however, the friction force is often observed to decrease at larger slip-velocities, suggesting that the bond formation cannot catch up. A decreasing friction force would change the tail of the velocity distribution of equation (9). We emphasize that the data we shall consider here does not reveal a consistent departure from an exponential tail at larger velocities.

As suggested from observations of individual cells [30], the singular transition of Coulomb friction when going from no motion to motion might not be fully representative of the substrate friction. In the following, we therefore consider an approximately linear friction for small velocities crossing exponentially over to a velocity-independent friction for larger velocites by using a friction term of the form $\boldsymbol{\psi}(\mathbf{v}) = -\alpha\tanh(v/w_0)\hat{\mathbf{v}}$. The characteristic speed w_0 determines the point of crossover to velocity-independent friction. Note that this friction would still result in an exponential speed distribution for larger speeds.

Table 1. Model parameters.

Symbol	Units	Description
λ_1	time	Relaxation time
λ_2	time	Retardation time
λ_m	time	Motility persistence time
ℓ_m	length	Motility length scale
β_m	length^4/time^2	Motility noise strength
η_0	mass/(length·time)	Total viscosity
α	length/time^2	Friction coefficient
w_0	length/time	crossover to constant friction

2.2. Equations of motion

The tissues, we consider, are confluent monolayers of cells residing on a substrate. The layers are taken to be incompressible such that the divergence of the local mean velocity vanishes and the projected area of each cell is conserved. We model the tissue dynamic by a momentum balance equation where cell motility is introduced via a persistent random forcing. From the considerations in the previous section, the interaction between tissue and substrate will be given by a friction term of the form $\boldsymbol{\psi}(\mathbf{v}) = -\alpha\tanh(v/w_0)\hat{\mathbf{v}}$

$$\frac{\partial \mathbf{v}}{\partial t} + (\mathbf{v}\cdot\nabla)\mathbf{v} = -\frac{1}{\rho}\nabla p + \frac{1}{\rho}\nabla\cdot\sigma + \boldsymbol{\psi}(\mathbf{v}) + \mathbf{m}, \tag{12}$$

$$0 = \nabla\cdot v \tag{13}$$

$$\frac{\partial \mathbf{m}}{\partial t} + (\mathbf{v}\cdot\nabla)\mathbf{m} = -\frac{1}{\lambda_m}\mathbf{m} + \boldsymbol{\phi}(\mathbf{x},t). \tag{14}$$

Here, ρ is the mean density, p is pressure and σ is the deviatoric stress tensor. The term $\mathbf{m}(\mathbf{x},t)$ is the force driving the cell motility, λ_m is a persistence time and $\boldsymbol{\phi}$ is filtered white Gaussian noise. Note that in contrast to the considerations above, the noise term, in the case of non-interacting motile cells, would lead to persistent random motion. Similar persistent random motion has been considered, for example, in [36, 37]. As each cell is a coherent body, there is a minimum length scale—similar to the cell size—below which the velocity field is approximately constant. We therefore impose a length scale ℓ_m on the random forcing by filtering the noise field $\boldsymbol{\xi}$ with a Gaussian function of

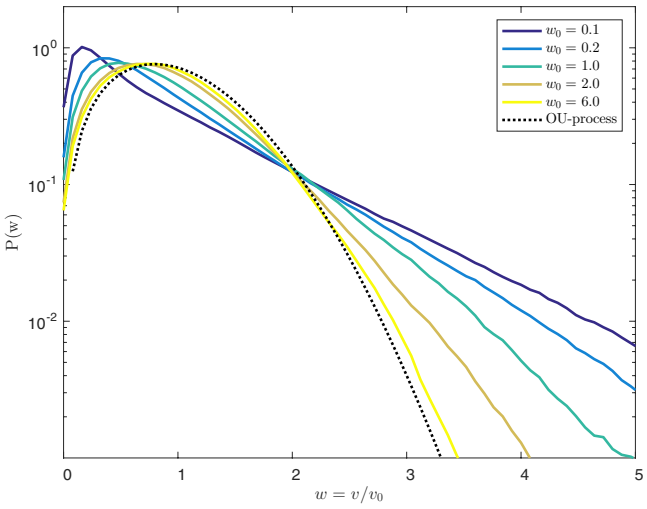

Figure 2. Comparison between the Ornstein–Uhlenbeck process and our continuum model of tissue dynamics. The numerical simulation is based on equations (17)–(21). For the large cross-over value, w_0, in the friction term, we go from a distribution with an exponential tail to a distribution with a Gaussian tail.

width ℓ_m and zero mean to obtain the filtered noise field $\boldsymbol{\phi}(\mathbf{x}, t)$:

$$\boldsymbol{\phi}(\mathbf{x}, t) = \frac{1}{2\pi\ell_m^2} \int \boldsymbol{\xi}(\mathbf{x}', t) \exp\left(-\frac{|\mathbf{x} - \mathbf{x}'|^2}{2\ell_m^2}\right) d\mathbf{x}'. \tag{15}$$

The strength of the white Gaussian noise field was taken to be $\langle \xi_i(\mathbf{x}, t)\xi_j(\mathbf{x}', t')\rangle = \beta_m \delta^{(2)}(\mathbf{x} - \mathbf{x}')\delta(t - t')\delta_{ij}$ where the indices i, j run over the spatial directions x, y. It follows that the filtered noise field will have an exponentially decaying spatial correlation:

$$\langle \phi_i(\mathbf{x}, t)\phi_j(\mathbf{x}', t')\rangle = \frac{\beta_m}{4\pi\ell_m^2} \exp\left(-\frac{|\mathbf{x} - \mathbf{x}'|^2}{4\ell_m^2}\right) \delta(t - t')\delta_{ij}. \tag{16}$$

We note that the cell motion is strongly over-damped (the flow occurs at negligible Reynolds numbers) and it is therefore safe to neglect the inertial terms on the left-hand side of equation (12).

2.3. Model parameters

The model described above has eight parameters, which we have listed in table 1. We can then use the viscosity η_0, along with the density ρ, the relaxation time λ_m and a characteristic length ℓ_m, to cast the model equations in a dimensionless form,

$$\nabla p = \nabla \cdot \sigma - a_\alpha \tanh(a_w v)\hat{\mathbf{v}} + \mathbf{m} \tag{17}$$

$$\nabla \cdot \mathbf{v} = 0 \tag{18}$$

$$\sigma + a_1 \frac{\partial \sigma}{\partial t} = 2\left(\gamma + a_2 \frac{\partial \gamma}{\partial t}\right) \tag{19}$$

$$\mathbf{m} + \frac{\partial \mathbf{m}}{\partial t} = \boldsymbol{\phi}(\mathbf{x}, t) \tag{20}$$

$$\langle \phi_i(\mathbf{x}, t)\phi_j(\mathbf{x}', t')\rangle = \frac{a_\beta}{4\pi} \exp\left(-\frac{|\mathbf{x} - \mathbf{x}'|^2}{4}\right) \delta(t - t')\delta_{ij}, \tag{21}$$

where we have defined the dimensionless control parameters:

$$a_1 = \frac{\lambda_1}{\lambda_m}, \quad a_2 = \frac{\lambda_2}{\lambda_m}, \quad a_\alpha = \frac{\rho}{\eta_0}\ell_m^2\alpha,$$
$$a_\beta = \left(\frac{\rho}{\eta_0}\right)^2 \lambda_m^3 \beta_m, \quad a_w = \frac{\ell_m}{\lambda_m w_0}. \tag{22}$$

That is, we have five parameters to fit by the numerical simulation of equations (17)–(21). From these five parameters, it is not possible to extract all the eight parameters in table 1. For example, we can only determine the ratio between the friction constant and the viscosity as well as the ratio between the viscosity and the noisy driving force. We note that we cannot explicitly determine the viscosity. In figure 2, we have computed the distribution of speed for different values of w_0 used in the friction term for typical tissue parameters. We see that for large w_0, we recover the Gaussian tail characteristic for the Ornstein–Uhlenbeck process, whereas, when w_0 is smaller than typical speeds in the tissue, we have an exponential tail in the speed distribution.

We apply our model to the experimental data on epithelial and endothelial tissue from [14, 38]. The model is simulated numerically using a pseudo-spectral method on a two dimensional (2D) periodic domain. The Fourier and inverse Fourier transforms in the spectral formulation are performed using the fast Fourier transform algorithm, and the non-linear terms are evaluated in real space. Time integration of the stress tensor and the noise term are performed using an exponential time differencing scheme [39]. In each time step, the velocity field and the pressure is found by a relaxation procedure. The periodic 2D computational domain consists of 256 × 256 grid points corresponding to a box of length ∼200 μm in physical units. The time step was ∼0.01 min in physical units. From the model parameters, we recover parameters with physical units for each cell type by matching the

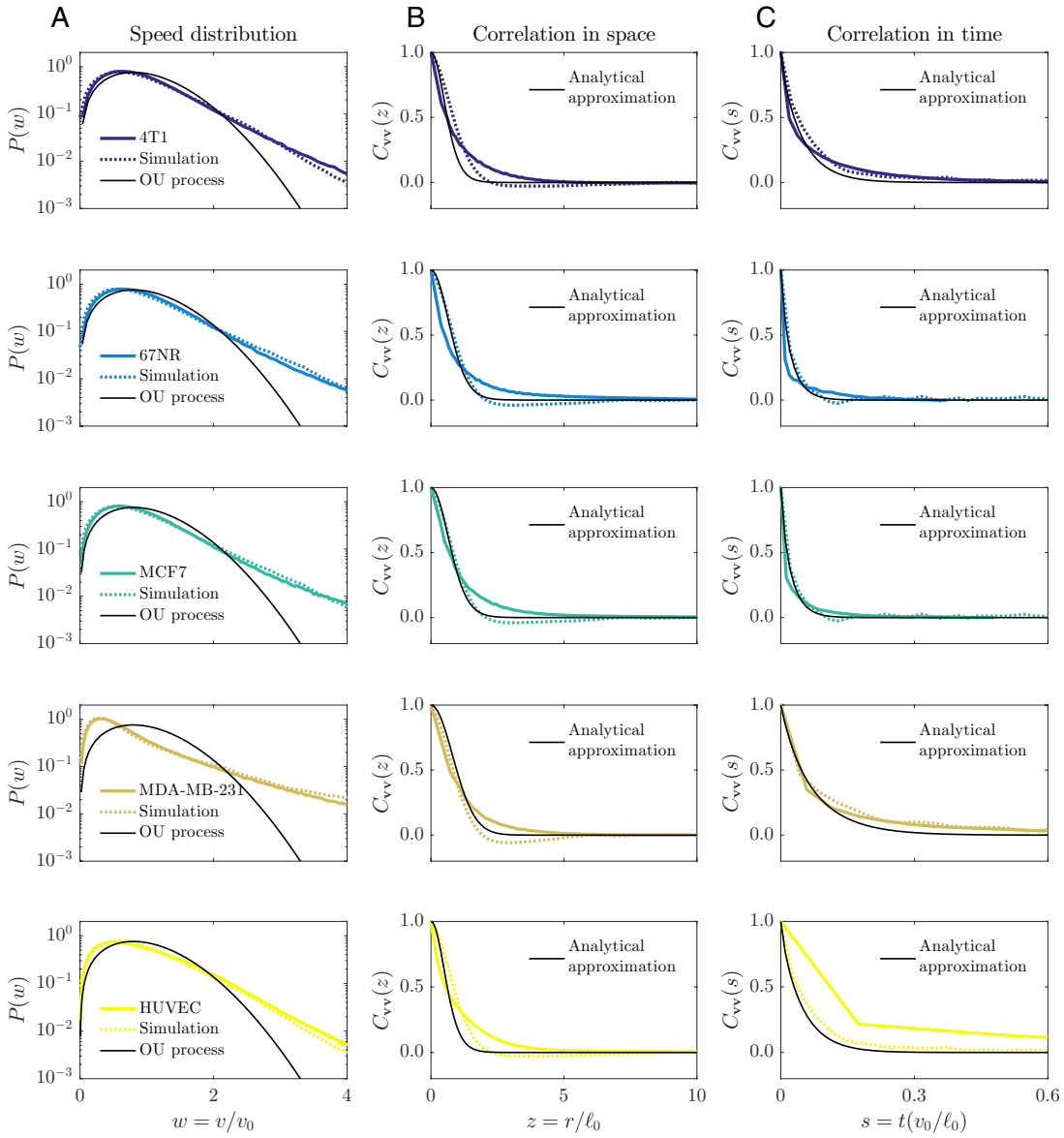

Figure 3. Comparison between model and experimental data. Experimentally measured statistical characteristics are plotted as solid colored lines, whereas statistical characteristics of the model fits are displayed as dashed lines. Speed, distance and time are rescaled by the mean speed v_0, the spatial correlation length ℓ_0 and the time scale ℓ_0/v_0 respectively. (A) The exponential tails of the speed distributions are captured by the model. We note, that the experimental and simulated speed distributions are very different from the result of an Ornstein–Uhlenbeck process (full black line), which results in a Gaussian tail. (B) The spatial correlation function of the model shows a negative dip which is not present in the data, but otherwise matches the experiments. The analytical correlation functions in the case of a drag term (calculated in section 2) (C) The temporal correlation functions are closely matched by the model.

simulation mean speed v_0 with the experimental mean speeds (listed in appendix A) and the simulation velocity correlation length ℓ_0 with the experimental velocity correlation length. Finally, the main constituent of biological tissue is water; we therefore do not consider the density ρ as a free parameter of the model.

3. Results

We fit the model by performing a parameter grid search and by choosing the parameters simultaneously resulting in the smallest relative squared error between the experimental $P^e(v)$ and simulated speed distribution $P^s(v)$, the spatial velocity correlation function (simulated $C^s_{vv}(r)$ and experimental $C^e_{vv}(r)$) and the temporal velocity correlation function (simulated $C^s_{vv}(t)$ and experimental $C^e_{vv}(t)$), i.e. the parameters that minimize the sum

$$\left\langle \left(\frac{P^e - P^s}{P^s} \right)^2 \right\rangle_v + \left\langle \left(\frac{C^e_{vv} - C^s_{vv}}{C^s_{vv}} \right)^2 \right\rangle_r + \left\langle \left(\frac{C^e_{vv} - C^s_{vv}}{C^s_{vv}} \right)^2 \right\rangle_t ,$$

where the averages are taken over the limited ranges shown in figure 3. We note that the choice of error function is somewhat arbitrary and that individual parts could have been weighted differently. Nonetheless, we believe that similar results would be obtained from related error functions. The set of best fit parameters for each cell type is listed in table 2 and follows from the limit of pure solid friction

Table 2. Fitted parameters for bulk cell motion.

Cell type	λ_1 (min)	λ_2 (min)	λ_m (min)	ℓ_m (μm)	$\alpha\,(\rho/\eta_0)$ (μm·min)$^{-1}$	$\beta_m\,(\rho/\eta_0)^2$ (min)$^{-3}$
4T1	1.6	0.4	7.8	10	0.002	0.003
67NR	2.9	0.7	7.1	12	0.001	0.001
MCF7	1.2	0.3	3.0	9	0.003	0.010
MDA-MB-231	2.2	0.2	4.3	7	0.015	0.125
HUVEC	1.6	0.4	7.8	10	0.002	0.003

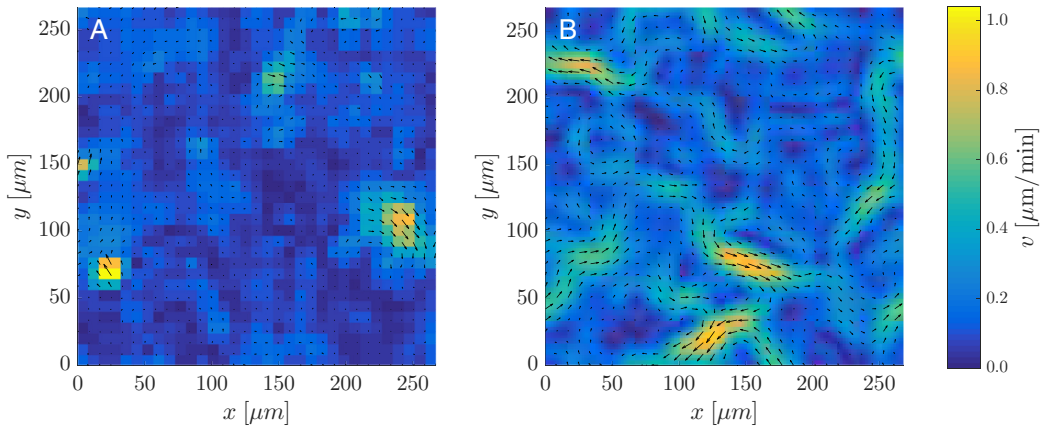

Figure 4. Bulk velocity fields. (A) Experiment. Human MCF7 cells during bulk motion. (B) Simulation. Velocity field of a simulation, where the speed distribution $P(v)$, the temporal velocity correlation $C_{vv}(t)$ and the spatial velocity correlation $C_{vv}(r)$ have been fitted to the experimentally measured data of the MCF7 cells.

also considered in [38]. The model reproduces, fairly accurately, the spatial and temporal velocity correlations—see figures 3(A)–(C) and where the results for both the epithelial and endothelial tissue is consistent with the findings in [38]. The choice of friction force in the model leads to an exponentially decaying tail of the speed distribution. Note that the only slight difference between the model and experiments is in the spatial correlation function, where the model has a slightly more pronounced dip than in the experimental data (see figure 3(B)). The spatial correlation in the model predominantly enters through the correlation length scale introduced by the structured noise (see equation (16)). The length scale of the noise dominates over the one introduced by the viscous forces. Below the length scale of the structured noise, our model slightly overestimates the spatial correlation, which is also apparent in figure 4 where indeed, locally, the correlation in the models seems stronger than in the experiments. Figure 4 shows an example of a velocity field obtained from a best fit together with a random zoom on an experimentally measured velocity field. In the experimental data, however, the spatial correlation is long ranged, probably due to stronger interaction forces between the neighboring cells (seen by the slightly slower decay in the velocity field in the experimental panel of figure 4). To model the cross-over between the small and large scale correlations more accurately, we would have to generalize further our visco-elastic terms.

Finally, we should mention that numerical simulations where the friction term is replaced by a drag term $-\alpha\mathbf{v}$ do not lead to a significant change in the correlation functions. The choice of a drag or a Coulomb friction mainly affects the speed distribution. The velocity correlation functions can be calculated analytically when advection of the noise field is neglected and when a drag term is used instead of a friction term (see appendix B). The resulting analytical correlation functions are displayed as black lines in figure 3 and closely resemble the simulations.

4. Conclusions and discussion

In a continuum model of tissue dynamics, we find that a solid friction term between cells and a substrate in a mono-layered tissue describes the exponential tail in the cell speed distribution fairly well. This is in contrast to many existing continuum and particle models, which typically consider a drag term linear in the velocity field and therefore a Gaussian tailed speed distribution. In addition to the experimental data considered here, a similar exponential tail has been observed, for example, for dilute suspensions of the MDA-MB-231 cell line [40]. Non-Gaussian tails have also been observed experimentally for other types of tissue [36, 37, 41]. To our knowledge, little is known about the cell–substrate dissipation process on the tissue scale, and it would be interesting to obtain firmer experimental knowledge on the appropriateness of either a linear drag or a Coulomb type friction. By modifying the frictional force to make a cross over between a drag-like friction at small velocities to Coulumb friction at larger velocities, our model can

further capture speed distributions with a Gaussian-like intermediate range, consistent with experimental observations [1].

The self-propulsion of cells in the proposed model incorporates a length scale and a persistence time of the local motility force field, which accounts for the finite extent of a single cell and for the tendency of a single cell to change its velocity in a certain time scale. Several papers have used related but more elaborate approaches, where the motility force field evolves in time due to some specified dynamics. Basan *et al* [42] proposed that the local motility force tends to align with the tissue velocity, and, combined with an assumption of cell locomotion being suppressed by neighbors, Zimmermann *et al* [43] were able to model the traction patterns observed experimentally in spreading epithelial tissue [44, 45]. Other authors have envisioned the polarization field as a 2D nematic liquid crystal [10, 13, 29], which allows for complex flow patterns with vortices and jets. In contrast to these existing models, the proposed motility evolution contains no assumptions of velocity–motility alignment or nematic behavior.

Including a motility force explicitly, as we have done in this paper, has the advantage that the local velocity need not be aligned with the local motility force. This behavior has been observed in an expanding monolayer, where the velocity and the local motility (traction) force under certain circumstances were anti parallel [45]. A natural next step is therefore to incorporate tissue boundaries in the proposed model, such that monolayer expansion and the generated tractions can be studied. This would also allow the model to be compared with, and used to study, the classical scratch-wound assay experiment [46–48], the observed fingering of tissue edges [48, 49] and the propagation of strain rate waves in spreading tissue [50].

Acknowledgments

The authors acknowledge financial support from the Danish Research Council DFF-4002-00099, from the Danish National Research Foundation DNRF116 and from the Villum Foundation grant Earth Patterns.

Appendix A. Cell cultures and experiments

The data used with our model are taken from [14, 38]. The mean speed and velocity correlation length observed in the experiments are listed below.

Table A1. Measured characteristics of experimental velocity fields in bulk experiments. The correlation length ℓ_0 was found by fitting a single exponential $C_{vv}(r) = e^{-r/\ell_0}$ to the spatial correlation functions displayed in figure 3.

Cell line	Mean speed v_0 (μm min^{-1})	Correlation length ℓ_0 (μm)
4T1	(0.27 ± 0.06)	(25.8 ± 0.9)
67NR	(0.13 ± 0.03)	(26.5 ± 1.1)
MCF7	(0.23 ± 0.02)	(19.6 ± 0.7)
MDA-MB-231	(0.7 ± 0.2)	(13.7 ± 0.4)
HUVEC	(0.5 ± 0.1)	(28.0 ± 0.1)

Appendix B. Analytical calculation of velocity correlation functions

In order to analytically calculate the velocity correlation functions of the model, we make two simplifications. We neglect the advection of the motility field $\mathbf{m}(\mathbf{x}, t)$ and we replace the non-linear friction term $-\alpha\hat{\mathbf{v}}$ with the linear drag term $-\alpha\mathbf{v}$. The simplified model equation system reads:

$$\nabla p = \nabla \cdot \sigma - \alpha\rho\mathbf{v} + \rho\mathbf{m} \qquad \text{Momentum balance with drag}$$

$$\nabla \cdot \mathbf{v} = 0 \qquad \text{Incompressibility}$$

$$\sigma + \lambda_1 \frac{\partial \sigma}{\partial t} = 2\eta_0 \left(\gamma + \lambda_2 \frac{\partial \gamma}{\partial t}\right) \qquad \text{Constitutive relation}$$

$$\mathbf{m} + \lambda_m \frac{\partial \mathbf{m}}{\partial t} = \lambda_m \phi(\mathbf{x}, t) \qquad \text{Motility evolution.}$$

The noise $\phi(\mathbf{x}, t)$ in the motility evolution is filtered white Gaussian noise satisfying:

$$\langle \phi_i(\mathbf{x}, t)\phi_j(\mathbf{x}', t')\rangle = \frac{\beta_m}{4\pi\ell_m^2} \exp\left(-\frac{|\mathbf{x} - \mathbf{x}'|^2}{4\ell_m^2}\right) \delta(t - t')\delta_{ij}. \tag{B.1}$$

Assuming that the initial stress, velocity and motility fields vanish $\sigma(\mathbf{x}, 0) = \mathbf{v}(\mathbf{x}, 0) = \mathbf{m}(\mathbf{x}, 0) = 0$, the Laplace- and Fourier-transformed velocity field $\tilde{v}_j(\mathbf{k}, s)$ can be isolated. Here, $\mathbf{k}$ is the Fourier transform variable, s is the Laplace transform variable and the index j runs over the spatial directions x, y. The real space, real time velocity field is then:

$$\begin{aligned} v_j(\mathbf{x}, t) &= \frac{1}{(2\pi)^2} \int d^2\mathbf{k}\, \frac{1}{2\pi i} \int_\Gamma ds\; e^{i\mathbf{k}\cdot\mathbf{x} + st} \tilde{v}_j(\mathbf{k}, s) \\ &= \frac{1}{(2\pi)^2} \int d^2\mathbf{k}\, \frac{1}{2\pi i} \int_\Gamma ds\, e^{i\mathbf{k}\cdot\mathbf{x} + st} f(k, s) \\ &\quad \times \left[\tilde{\phi}_j(\mathbf{k}, s) - k_j \frac{k_x\tilde{\phi}_x(\mathbf{k}, s) + k_y\tilde{\phi}_y(\mathbf{k}, s)}{k^2}\right], \end{aligned}$$

where Γ indicates the integration path in the complex plane for the inverse Laplace transform, and we have defined:

$$f(k, s) = \frac{1}{\left(a_\alpha + \frac{a_2}{a_1}k^2\right)} \frac{\left(s + \frac{1}{a_1}\right)}{(s + 1)\left(s + \frac{a_\alpha + k^2}{a_\alpha a_1 + a_2 k^2}\right)}. \tag{B.2}$$

The velocity component correlation is proportional to:

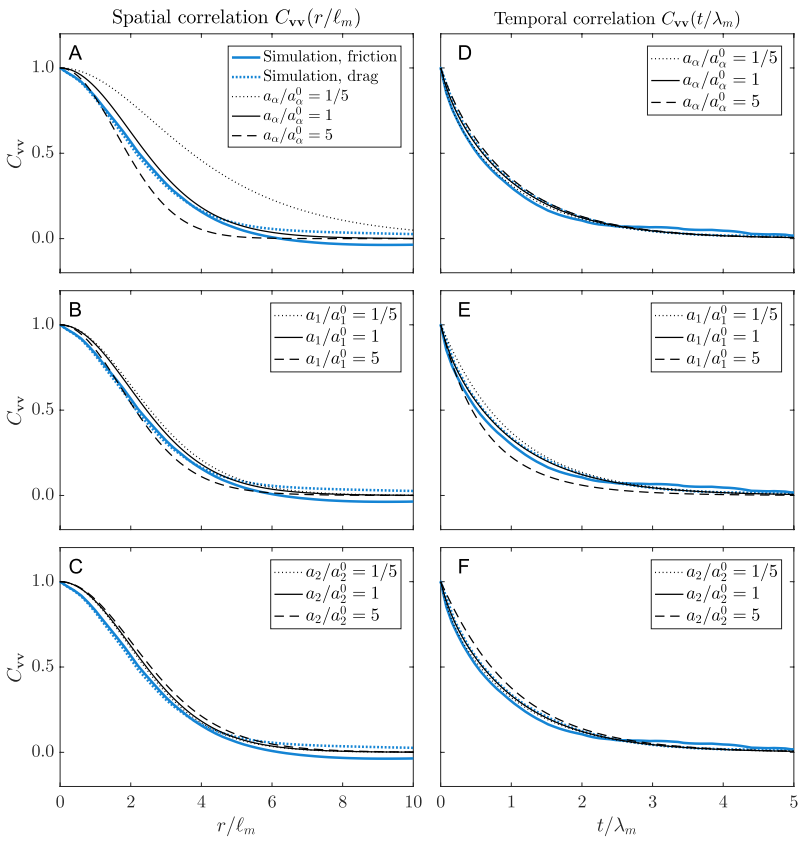

Figure B1. Analytically calculated correlation functions. The correlation functions obtained from simulations with friction (full blue line) and drag (dotted blue line) are very similar and both well described by the analytically calculated correlation function (full black line). The simulations shown here correspond to the case of 4T1 cells, and have the parameters $(a_\alpha^0, a_1^0, a_2^0)$. Panels (A)–(C) show the spatial correlation function when the three control parameters a_α, a_1 and a_2 are varied. Only a_α has a significant influence on the correlation function. Panels (B)–(D) show the temporal correlation function when the three control parameters are varied. The temporal correlation is very insensitive to the parameters.

$$
\begin{aligned}
&\left\langle v_i(\mathbf{x},t)v_j(\mathbf{x}',t')\right\rangle \\
&= \frac{1}{(2\pi)^2}\frac{1}{(2\pi i)^2}\int d^2\mathbf{k}\int d^2\mathbf{k}'\int_\Gamma ds \\
&\quad \int_{\Gamma'} ds'\; e^{i\mathbf{k}\cdot\mathbf{x}+i\mathbf{k}'\cdot\mathbf{x}'+st+s't'} f(k,s)f(k',s') \\
&\quad \left\langle \left[\tilde{\phi}_j(\mathbf{k},s) - k_j\frac{k_x\tilde{\phi}_x(\mathbf{k},s)+k_y\tilde{\phi}_y(\mathbf{k},s)}{k^2}\right]\right. \\
&\times \left.\left[\tilde{\phi}_j(\mathbf{k}',s') - k_j'\frac{k_x'\tilde{\phi}_x(\mathbf{k}',s')+k_y'\tilde{\phi}_y(\mathbf{k}',s')}{k'^2}\right]\right\rangle \\
&\quad \propto \int d^2\mathbf{k}\int_\Gamma ds\int_{\Gamma'} ds'\; e^{i\mathbf{k}\cdot(\mathbf{x}-\mathbf{x}')+st+s't'} \\
&\quad \frac{f(k,s)f(k,s')}{s+s'}e^{-k^2}\left[\delta_{ij}-\frac{k_ik_j}{k^2}\right]. \qquad \text{(B.3)}
\end{aligned}
$$

We note that the term e^{-k^2} is a result of the noise being filtered. If ϕ had been white Gaussian noise, the term would not have been present.

The velocity correlation function $C_{vv}(r,\tau)$ of $r = |\mathbf{x}-\mathbf{x}'|$ and $\tau = t-t' > 0$ is then proportional to:

$$
\begin{aligned}
C_{vv}(r,\tau) &\propto \langle v_x(\mathbf{x},t)v_x(\mathbf{x}',t')\rangle + \langle v_y(\mathbf{x},t)v_y(\mathbf{x}',t')\rangle \\
&\propto \int d^2\mathbf{k}\int_\Gamma ds\int_{\Gamma'} ds'\; e^{i\mathbf{k}\cdot(\mathbf{x}-\mathbf{x}')+st+s't'}\frac{f(k,s)f(k,s')}{s+s'}e^{-k^2} \\
&\propto \int_0^\infty k\,J_0(kr)\,dk\int_\Gamma ds\int_{\Gamma'} ds'\; e^{st+s't'}\frac{f(k,s)f(k,s')}{s+s'}e^{-k^2} \\
&= \int_0^\infty k\,J_0(kr)\,dk\int_0^{t'} dt_1\, f(k,t-t_1)f(k,t'-t_1)e^{-k^2},
\end{aligned}
$$

where the Fourier transform has been turned into a Hankel transform and $J_0(kr)$ is the zeroth order Bessel function of the first kind. The function $f(k,t)$ can be found analytically by applying the inverse Laplace transform to equation (B.2) and also the integral over t_1 can be performed analytically.

Neglecting the transient behavior $(t,t' \gg 0)$, we find the spatial correlation function for equal times $\tau = t-t' = 0$:

$$
\begin{aligned}
&C_{vv}(r) = C_{vv}(r,0) \\
&\propto \int_0^\infty dk\,\frac{k\,J_0(kr)\,e^{-k^2}}{\left(a_\alpha+\frac{a_2}{a_1}k^2\right)\left(a_\alpha+k^2\right)}\frac{(1+a_1)a_\alpha+\left(a_1+\frac{a_2}{a_1}\right)k^2}{\left((1+a_1)a_\alpha+(1+a_2)k^2\right)}, \qquad \text{(B.4)}
\end{aligned}
$$

and the temporal correlation function for a fixed point in space $r = |\mathbf{x} - \mathbf{x}'| = 0$:

$$C_{vv}(\tau) = C_{vv}(0,\tau) \propto \int_0^\infty dk \, \frac{k\, e^{-k^2}}{\left(a_\alpha + \frac{a_2}{a_1}k^2\right)^2} \left[-\left(\frac{1}{2s_a} f_1(k)^2 + \frac{1}{s_a + s_b} f_1(k) f_2(k)\right) e^{\tau s_a} - \left(\frac{1}{2s_b} f_2(k)^2 + f_1(k) f_2(k) \frac{1}{s_a + s_b} e^{\tau s_b}\right)\right]. \tag{B.5}$$

Here, we have denoted the two simple poles of $f(k,s)$ as s_a, s_b and defined the two functions $f_1(k), f_2(k)$:

$$s_a = -1 \qquad s_b = -\frac{a_\alpha + k^2}{a_\alpha a_1 + a_2 k^2} \qquad f_1(k) = \frac{s_a + \frac{1}{a_1}}{s_a - s_b} \qquad f_2(k) = \frac{s_b + \frac{1}{a_1}}{s_b - s_a}. \tag{B.6}$$

The integral over k in equations (B.4) and (B.5) was performed numerically and the resulting normalized correlation functions are plotted in figure B1 for various parameter combinations.

ORCID iDs

Lene Broeng Oddershede https://orcid.org/0000-0003-2923-2844
Joachim Mathiesen https://orcid.org/0000-0002-5621-5487

References

[1] Sepúlveda N, Petitjean L, Cochet O, Grasland-Mongrain E, Silberzan P and Hakim V 2013 Collective cell motion in an epithelial sheet can be quantitatively described by a stochastic interacting particle model *PLoS Comput. Biol.* **9** e1002944
[2] Arboleda-Estudillo Y, Krieg M, Stühmer J, Licata N A, Muller D J and Heisenberg C-P 2010 Movement directionality in collective migration of germ layer progenitors *Curr. Biol.* **20** 161–9
[3] Szabó B, Szöllösi G J, Gönci B, Jurányi Z, Selmeczi D and Vicsek T 2006 Phase transition in the collective migration of tissue cells: experiment and model *Phys. Rev.* E **74** 061908
[4] Méhes E and Vicsek T 2014 Collective motion of cells: from experiments to models *Integr. Biol.* **6** 831–54
[5] Graner F and Glazier J A 1992 Simulation of biological cell sorting using a two-dimensional extended Potts model *Phys. Rev. Lett.* **69** 2013–6
[6] Szabó A, Ünnep R, Méhes E, Twal W O, Argraves W S, Cao Y and Czirók A 2010 Collective cell motion in endothelial monolayers *Phys. Biol.* **7** 046007
[7] Albert P J and Schwarz U S 2016 Dynamics of cell ensembles on adhesive micropatterns: bridging the gap between single cell spreading and collective cell migration *PLoS Comput. Biol.* **12** e1004863
[8] Farhadifar R, Röper J-C, Aigouy B, Eaton S and Jülicher F 2007 The influence of cell mechanics, cell–cell interactions, and proliferation on epithelial packing *Curr. Biol.* **17** 2095–104
[9] Aland S, Hatzikirou H, Lowengrub J and Voigt A 2015 A mechanistic collective cell model for epithelial colony growth and contact inhibition *Biophys. J.* **109** 1347–57
[10] Lee P and Wolgemuth C W 2011 Crawling cells can close wounds without purse strings or signaling *PLoS Comput. Biol.* **7** e1002007
[11] Bittig T, Wartlick O, Kicheva A, González-Gaitán M and Jölicher F 2008 Dynamics of anisotropic tissue growth *New J. Phys.* **10** 063001
[12] Ranft J, Basan M, Elgeti J, Joanny J-F, Prost J and Jülicher F 2010 Fluidization of tissues by cell division and apoptosis *Proc. Natl Acad. Sci.* **107** 20863–8
[13] Doostmohammadi A, Thampi S P, Saw T B, Lim C T, Ladoux B and Yeomans J M 2015 Celebrating soft matter's 10th anniversary: cell division: a source of active stress in cellular monolayers *Soft Matter* **11** 7328–36
[14] Rossen N S, Tarp J M, Mathiesen J, Jensen M H and Oddershede L B 2014 Long-range ordered vorticity patterns in living tissue induced by cell division *Nat. Commun.* **5** 5720
[15] Köpf M H and Pismen L M 2013 A continuum model of epithelial spreading *Soft Matter* **9** 3727
[16] Banerjee S, Utuje K J C and Marchetti M C 2015 Propagating stress waves during epithelial expansion *Phys. Rev. Lett.* **114** 228101
[17] Arciero J C, Mi Q, Branca M F, Hackam D J and Swigon D 2011 Continuum model of collective cell migration in wound healing and colony expansion *Biophys. J.* **100** 535–43
[18] Cochet-Escartin O, Ranft J, Silberzan P and Marcq P 2014 Border forces and friction control epithelial closure dynamics *Biophys. J.* **106** 65–73
[19] Lim C T, Zhou E H and Quek S T 2006 Mechanical models for living cells—a review *J. Biomech.* **39** 195–216
[20] Kasza K E, Rowat A C, Liu J, Angelini T E, Brangwynne C P, Koenderink G H and Weitz D A 2007 The cell as a material *Curr. Opin. Cell Biol.* **19** 101–7
[21] Zhu C, Bao G and Wang N 2000 Cell mechanics: mechanical response, cell adhesion, and molecular deformation *Annu. Rev. Biomed. Eng.* **2** 189–226
[22] Verdier C, Etienne J, Duperray A and Preziosi L 2009 Review: rheological properties of biological materials *C. R. Phys.* **10** 790–811
[23] Harris A R, Peter L, Bellis J, Baum B, Kabla A J and Charras G T 2012 Characterizing the mechanics of cultured cell monolayers *Proc. Natl Acad. Sci.* **109** 16449–54
[24] Guevorkian K, Colbert M-J, Durth M, Dufour S and Brochard-Wyart F 2010 Aspiration of biological viscoelastic drops *Phys. Rev. Lett.* **104** 218101
[25] Forgacs G, Foty R A, Shafrir Y and Steinberg M S 1998 Viscoelastic properties of living embryonic tissues: a quantitative study *Biophys. J.* **74** 2227–34
[26] Wang Y and Insana M F 2013 Viscoelastic properties of rodent mammary tumors using ultrasonic shear-wave imaging *Ultrason. Imaging* **35** 126–45
[27] Larson R G 1998 *The Structure and Rheology of Complex Fluids* 1st edn (New York: Oxford University Press)
[28] Galle J, Loeffler M and Drasdo D 2005 Modeling the effect of deregulated proliferation and apoptosis on the growth dynamics of epithelial cell populations *in vitro Biophys. J.* **88** 62–75
[29] Doostmohammadi A, Adamer M F, Thampi S P and Yeomans J M 2016 Stabilization of active matter by flow-vortex lattices and defect ordering *Nat. Commun.* **7** 10557
[30] Gardel M L, Sabass B, Ji L, Danuser G, Schwarz U S and Waterman C M 2008 Traction stress in focal adhesions correlates biphasically with actin retrograde flow speed *J. Cell Biol.* **183** 999–1005
[31] Srinivasan M and Walcott S 2009 Binding site models of friction due to the formation and rupture of bonds: state-function formalism, force-velocity relations, response to slip velocity transients, and slip stability *Phys. Rev.* E **80** 046124

[32] Gail M H and Boone C W 1970 The locomotion of mouse fibroblasts in tissue culture *Biophys. J.* **10** 980–93
[33] Dunn G A and Brown A F 1987 A unified approach to analysing cell motility *J. Cell Sci.* **1987** 81–102
[34] Hayakawa H 2005 Langevin equation with coulomb friction *Physica* D **205** 48–56
[35] Dieterich J H 1979 Modeling of rock friction: 1. Experimental results and constitutive equations *J. Geophys. Res.* **84** 2161–8
[36] Selmeczi D, Mosler S, Hagedorn P H, Larsen N B and Flyvbjerg H 2005 Cell motility as persistent random motion: theories from experiments *Biophys. J.* **89** 912–31
[37] Takagi H, Sato M J, Yanagida T and Ueda M 2008 Functional analysis of spontaneous cell movement under different physiological conditions *PLoS One* **3** e2648
[38] West A-K V, Wullkopf L, Christensen A, Leijnse N, Tarp J M, Mathiesen J, Erler J T and Oddershede L B 2017 Dynamics of cancerous tissue correlates with invasiveness *Sci. Rep.* **7** 43800
[39] Cox S M and Matthews P C 2002 Exponential time differencing for stiff systems *J. Comput. Phys.* **176** 430–55
[40] Czirók A, Schlett K, Madarász E and Vicsek T 1998 Exponential distribution of locomotion activity in cell cultures *Phys. Rev. Lett.* **81** 3038–41
[41] Upadhyaya A, Rieu J-P, Glazier J A and Sawada Y 2001 Anomalous diffusion and non-Gaussian velocity distribution of Hydra cells in cellular aggregates *Physica* A **293** 549–58
[42] Basan M, Elgeti J, Hannezo E, Rappel W-J and Levine H 2013 Alignment of cellular motility forces with tissue flow as a mechanism for efficient wound healing *Proc. Natl Acad. Sci.* **110** 2452–9
[43] Zimmermann J, Camley B A, Rappel W-J and Levine H 2016 Contact inhibition of locomotion determines cell–cell and cell–substrate forces in tissues *Proc. Natl Acad. Sci.* **113** 2660–5
[44] Trepat X, Wasserman M R, Angelini T E, Millet E, Weitz D A, Butler J P and Fredberg J J 2009 Physical forces during collective cell migration *Nat. Phys.* **5** 426–30
[45] Kim J H *et al* 2013 Propulsion and navigation within the advancing monolayer sheet *Nat. Mater.* **12** 856–63
[46] Rosen P and Misfeldt D S 1980 Cell density determines epithelial migration in culture *Proc. Natl Acad. Sci.* **77** 4760–3
[47] Farooqui R and Fenteany G 2005 Multiple rows of cells behind an epithelial wound edge extend cryptic lamellipodia to collectively drive cell-sheet movement *J. Cell Sci.* **118** 51–63
[48] Poujade M, Grasland-Mongrain E, Hertzog A, Jouanneau J, Chavrier P, Ladoux B, Buguin A and Silberzan P 2007 Collective migration of an epithelial monolayer in response to a model wound *Proc. Natl Acad. Sci.* **104** 15988–93
[49] Reffay M, Petitjean L, Coscoy S, Grasland-Mongrain E, Amblard F, Buguin A and Silberzan P 2011 Orientation and polarity in collectively migrating cell structures: statics and dynamics *Biophys. J.* **100** 2566–75
[50] Serra-Picamal X, Conte V, Vincent R, Anon E, Tambe D T, Bazellieres E, Butler J P, Fredberg J J and Trepat X 2012 Mechanical waves during tissue expansion *Nat. Phys.* **8** 628–34